Base free oxidation of 1,6-hexanediol to adipic acid over supported noble metal mono- and bimetallic catalysts

M. Mounguengui-Diallo, F. Vermersch, N. Perret, C. Pinel, M. Besson

Base free oxidation of 1,6-hexanediol to adipic acid over supported noble metal mono- and bimetallic catalysts

Modibo Mounguengui-Diallo, François Vermersch, Noémie Perret, Catherine Pinel, Michèle Besson*

Univ Lyon, Univ Claude Bernard, CNRS, IRCELYON, UMR5256, Institut de recherches sur la catalyse et l'environnement de Lyon, 2 Avenue Albert Einstein, 69626 Villeurbanne, France

1,6-Hexanediol is an emerging building-block chemical, which may be derived from biomass and can produce adipic acid for the synthesis of polymers. A series of supported Pt, Bi-Pt, Au, Pd, Au-Pd, and Au-Pt catalysts were prepared and evaluated in the aerobic oxidation of 1,6-hexanediol to adipic acid in aqueous solution without the addition of a base or an acid. The influences of various molar ratios of the metals in the bimetallic systems and the support (C, ZrO_2) were studied. Under the conditions used, bismuth did not promote the catalytic perfor-mance of Pt catalysts. On the other hand, formation of an alloy of Au-Pd or Au-Pt made the catalysts very effective. A yield of adipic acid of ca. 96% was achieved at 70 °C under 40 bar of air over the Au-Pt catalyst supported on zirconia with a Au/Pt molar ratio of about 1. Recycling tests revealed the possibility to use the catalyst up to 6 times without significant changes in its catalytic performance.

1. Introduction

Adipic acid is an important monomer, primarily used in the manufacture of nylon 6,6 in its fiber and resin forms. Other applications include polyurethanes, adipic esters as plasticizers in PVC, lubricants, food and cosmetic additives [1,2]. The annual world production was almost 2.8 million metric tons in 2014 and it is expected to further increase at a compound annual grow rate of more than 3% in the next few years [3,4]. It is mostly obtained from petroleum-based feedstocks through the oxidation of cyclohexane to produce a cyclohexanol-cyclohexanone mixture, known as KA Oil, which is subsequently oxidized to adipic acid with an excess of nitric acid. Despite progress in recovery and reuse [5] one drawback of this route is the production of the greenhouse gas N_2O as by-product [6]. Alternative catalytic petrochemical routes [2] include the oxidation of cyclohexene with hydrogen peroxide [7–11], of cyclohexane with molecular oxygen [12–14], of cyclohexanol/one with air [15–17] or hydrogen peroxide [18,19], or the double hydroformylation of 1,3-butadiene followed by oxidation [20].

The manufacture of bio-based adipic acid has emerged as an alternative to the petrochemical process [2,3,21,22]. For instance, Rennovia claimed a two-step catalytic process starting with the hydrogenation of 2,5-furandicarboxylic acid to tetrahydrofuran-2,5-dicarboxylic acid (yield of 88%) followed by ring-opening to adipic acid (yield of 99%), using acetic acid as solvent [23]. Rennovia also disclosed a patent for the conversion of glucose to adipic acid, involving selective catalytic aerobic oxidation of glucose to glucaric acid in water (66% yield over Pt/SiO_2), that further undergoes hydrodeoxygenation to adipic acid in acetic acid using $PdRh/SiO_2$ and a halogen source (89% yield) [24,25]; the process is currently in its development stage. Several companies (Verdezyne, BioAmber, Genomatica among others) are developing fermentation routes of glucose or fatty acids to adipic acid [26]. Combined biological-chemical processes have also been proposed using the carbohydrate fractions of lignocellulosic biomass as feedstock [27–30]. Bio-based *cis,cis*-muconic acid is then catalytically hydrogenated to adipic acid over Pt/C [28,30], RuPt nanoparticles [29], or Ni/Al_2O_3 [31] with excellent yield; but the main drawback is associated to the difficulty of initial separation and purification of muconic acid [21]. Another pathway is a two-step reaction with upgrading of levulinic acid-derived γ-valerolactone to pentenoic acid isomers on a silica/alumina catalyst and subsequent conversion to adipic acid on a palladium acetate catalyst in the presence of CO and water [2,21].

An interesting bio-based route to produce adipic acid could also be via the oxidation of bio-1,6-hexanediol (HDO). The synthesis of bio-HDO has been widely studied using several catalytic chemical pathways: (i) the selective ring opening/hydrogenolysis of 2,5- tetrahydrofurandimethanol (synthesized from 2,5-hydroxymethylfurfural) [32–35], (ii) the selective hydrogenolysis of intermediate

* Corresponding author.
E-mail address: michele.besson@ircelyon.univ-lyon1.fr (M. Besson).

tetrahydropyran-2-methanol [34,36,37], or its sequential dehydration/hydration/hydrogenation [38], (iii) hydrogenolysis of sorbitol [39], or (iv) hydrogenation of levoglucosenone [40,41]. However, overall yields were still moderate (25%–40%).

Conversion of 1,6-HDO to adipic acid was previously claimed using biological oxidation [42]. However, catalytic oxidation of alcohols or aldehydes with molecular oxygen using noble metal heterogeneous catalysts is also possible [43–47]. The application of this method for the oxidation of α,ω-diols in aqueous solution with base has been investigated previously. The oxidation of a 0.1 M HDO in a 1 M NaOH aqueous solution over Au/C catalyst gave a 97% sodium adipate yield [45]. A Pt/C catalyst in 0.35 M acetic acid yielded 85% adipic acid after 24 h of reaction at 70 °C under 10 bar O_2, and using a molar substrate/metal ratio of 100 [43,44]. The advantage of Pt is that it can operate in neutral or acidic medium compared to gold-only catalyst formulations that require the use of a base [48]. However, rapid deactivation of the monometallic catalyst may occur by over-oxidation of the metal or by strongly adsorbed species on the catalyst surface [44,49].

The improvement brought by the addition of a second metal has been previously demonstrated for several reactions. The addition of Bi to noble metal enhances the resistance to deactivation by oxygen and may avoid the use of a base [48,50,51]. A Pt-Bi/C catalyst yielded 98% of adipic acid compared to only 46% over Pt/C after 36 h of reaction at 55 °C under 0.2 bar O_2 [46]. Conversely, (Pt-Sn/C) decreased adipic acid yield [52]. In fact, one of the difficulties of using bimetallic catalysts is that their structure can evolve over time during catalytic reaction, and in the case of Pt-Sn/C, the lower production of adipic acid has been linked to the formation of a Pt-Sn alloy [52]. The alloying of Pd or Pt with Au has been shown in recent years to enhance significant activity and stability [53–58]. Supported Pt, Au, Pd and bimetallic catalysts have been claimed to oxidize aqueous solution of 0.1 M 1,6-HDO to adipic acid with yields up to 99% at 140–160 °C in vials under pressure [47]. Independently of the metal used, the support may influence the catalytic performance. Even if most of the works for this catalytic reaction were carried out on active carbon support, the main drawback of this material is often its large surface area and its microporous volume that may lead to the significant adsorption of reaction products [44]. This is the reason why mesoporous ZrO_2 will be used as support.

The objective of this work was to perform the catalytic oxidation of 1,6-hexanediol into adipic acid and to compare the catalytic activity and selectivity in neutral medium of the promising C and ZrO_2 supported- Pt-Bi and Pt-Au and Pd-Au systems.

2. Experimental

2.1. Catalyst preparation

The supports used were activated carbon (CECA L3S, 900 $m^2 g^{-1}$, microporous) and ZrO_2 (MEL Chemicals, XZO 632/18, 132 $m^2 g^{-1}$, mesoporous, average pore diameter 9 nm).

The supported Pt/C and Pt/ZrO_2 catalysts were prepared by wet impregnation of the support [59]. An aqueous solution of H_2PtCl_6 (Sigma-Aldrich, 99% purity) containing the required amount of Pt was added dropwise under stirring to an aqueous suspension of the support under N_2 bubbling at room temperature. After 5 h, the slurry was cooled down in an ice bath and 50 mL of a 37 wt% formaldehyde solution was added, and then 20 mL of a 30 wt% KOH solution. After stirring under N_2 overnight, the solid was filtered and washed with water until neutrality of the filtrate. The catalysts were dried under N_2 at 70 °C overnight.

The Pt–Bi/C and Pt–Bi/ZrO_2 bimetallic catalysts were prepared from the monometallic catalysts via a surface redox reaction ensuring the deposition of bismuth on platinum, using $BiONO_3$ or $BiNO_3$,$5H_2O$ salts and glucose as reducing agent [50,59–61]. The monometallic Pt/C or Pt/ZrO_2 catalyst was suspended in an aqueous solution of glucose (glucose/Pt = 790). An appropriate amount of $BiONO_3$ or $BiNO_3$,$5H_2O$ corresponding to the targeted loading was dissolved in 2 M HCl and was added into the suspension under nitrogen atmosphere. The pH was then increased to 9 by addition of NaOH. Afterwards, the catalysts were filtered, washed, and dried under N_2 at 70 °C overnight.

The Pt-Au and Pd-Au catalysts supported on ZrO_2 were prepared by co-wet impregnation and $NaBH_4$ reduction [62]. In a three-necked flask of 1L the support was introduced in 500 mL of deionized water with mechanical stirring and bubbling of N_2. An aqueous solution of $HAuCl_4$ and H_2PtCl_6 (or $PdCl_2$) corresponding to the desired metal amounts was added over a period of 1 h (yellow color) with moderate stirring (400 rpm). The suspension was then cooled in an ice bath and a solution of $NaBH_4$ (20 mol. eq.) was added dropwise with vigorous stirring (800 rpm), which caused a sharp change of color towards black. After an additional 3 h-stirring at 400 rpm, the solid was filtered, washed until a negative test with $AgNO_3$, and dried under N_2 at 70 °C. Monometallic catalysts were prepared using the same protocol.

2.2. Catalysts characterization

The X-ray diffraction (XRD) patterns were recorded on a D8 Advance A25 diffractometer (Bruker) using a CuKα source (λ = 1.54184 Å). The crystalline phases were identified by reference to the JCPDS data files. The average crystallite size of the metal particles was calculated from line broadening according to Scherrer's equation using EVA and TOPAS software.

The metal loadings of the catalysts were determined by Inducted Coupled Plasma-Optical Emission Spectroscopy (ICP-OES) on a Activa Jobin-Yvon instrument. Prior to the analysis, the solids were solubilized in a mixture of H_2SO_4 and HNO_3 at 250–300 °C, and then in aqua regia at 150–200 °C.

Transmission Electron Microscopy (TEM) and energy dispersive X-ray spectroscopy (EDX) measurements were performed using a JEOL 2010 instrument operated at an accelerating voltage of 200 kV. The sample for TEM was prepared by ultrasonic dispersion in ethanol. A drop of dispersed catalyst was deposited onto the carbon-coated copper grid and the solvent was evaporated in air at room temperature. EDX was used to observe the composition of the catalysts.

2.3. HDO oxidation catalytic test

The catalytic oxidation reactions were carried out in a 300 mL batch reactor (Hastelloy) equipped with a magnetically driven gas inducing stirrer. The substrate (1,6-hexanediol, Alfa Aesar, 97%) (1 M, 2.77 g in 150 mL of ultra-pure water) and the appropriate amount of catalyst that corresponds to a HDO/metal molar ratio of 100 were introduced into the reactor. After sealing and purging the reactor with Ar, the suspension was heated to 70 °C, pressurized to 40 bar with air, and stirred at 1200 rpm, which corresponds to time zero. During the reaction, liquid samples were taken regularly via a sample diptube connected to a valve. After reaction, the autoclave was cooled and the catalyst was recovered by filtration through PVDF membrane (0.45 μm).

Recycling tests were also performed. After an experiment, the used catalyst was filtered on a PVDF membrane (0.45 μm), washed with water, dried at 70 °C under N_2, and reused without reactivation. A loss of ca. 10% of the catalyst mass was unavoidable during this process. To perform the experiment with comparable mass of catalyst, the lost solid was replaced by part of the used catalyst of another experiment performed under the same conditions.

2.4. Product analysis

Liquid samples were analyzed using a HPLC Shimadzu-10A equipped with Photodiode Array (PDA) and differential refraction (RI) detectors in series, after filtration through a 0.45 μm PVDF membrane and dilution by a factor 20. Product separation was carried out with a

Phenomenex Rezex ROA Acid H^+ column thermostated at 65 °C and with a 10 mM H_2SO_4 (0.6 mL min^{-1}) mobile phase. The retention times and the calibration curves for 6-hydroxyhexanoic acid (HA) and adipic acid (DA) were determined by injecting known concentrations of standard chemicals. 6-Hydroxyhexanal (ALD) and 6-oxohexanoic acid (AA) are not commercially available and were attributed to two other peaks, according to the order of appearance during the reaction. The lactone product of HDO (ε-caprolactone) exhibited the same retention time as HA. If formed, it should be hydrolyzed in water to 6-hydroxyhexanoic acid whatever the pH. Under similar reaction conditions, Ide et al. [44] also did not detect the formation of the lactone during oxidation of HDO over Pt/C or Pt-Bi/C catalysts. Therefore, we considered that it was not formed during the reaction.

The total organic carbon (TOC) in solution was measured using a TOC analyzer (Shimadzu TOC-V_{CSH} equipped with an ASI-automatic sampler). The carbon balance calculated from HPLC analysis was compared to the measured TOC values to verify the accuracy of the HPLC analysis. These values were further compared to the initial TOC value to check the possible adsorption on the catalytic solids or the degradation to gaseous products. The possible metal leaching of the catalyst was checked by ICP-OES of the final liquid reaction medium.

No conversion of HDO was observed in the blank test in the absence of either C or ZrO_2 support or a catalyst, after 5 h of reaction under the selected reaction conditions. The supports did not show any activity. The selectivity to a specific product was defined as moles of that product divided by the moles of all formed products.

3. Results and discussion

3.1. Supported Pt and Pt-Bi catalysts

Powder XRD patterns of the carbon-supported Pt and Pt-Bi catalysts recorded in the 2θ range of 10–80° are shown in Fig. S1. The determined metal loadings of the catalysts, the corresponding Bi/Pt molar ratios, and the determined average crystallite size of platinum are provided in Table 1.

The XRD pattern of $Pt_{3.7}$/C (Fig. S1) showed diffraction peaks observed around 2θ = 40°, 45°, and 67° that correspond to the (111), (200), and (222) planes of the face-centered cubic structure (fcc) of platinum (JCPDS 04-001-0112). The prominent broad bands centered at approximately 2θ = 27° and 43° are attributed to amorphous carbon (JCPDS 00-23-0064). No peak characteristic of Bi species was observed, in agreement with the literature on Pt-Bi catalysts which shows that Bi species is usually not detectable by XRD over these Pt-Bi systems [51,61]. The lattice constant found for Pt was not influenced by the deposition of Bi whatever the Bi content (3.93 Å), which indicated that bismuth was not inserted in the framework of Pt and excluded the formation of Pt-Bi alloy by this preparation procedure. The average metal crystallite size of Pt in $Pt_{3.7}$/C was ca. 4 nm, it increased slightly with the deposition of increasing amounts of Bi (Table 1). Indeed, the deposition of Bi over noble metals such as Pt or Pd may lead to particle growth, depending on the method of preparation [60,61].

$Pt_{3.7}$/C and the series of Bi-modified catalysts were evaluated in the

Table 1
Characterization of supported Pt and Bi-Pt catalysts.

Catalyst	Bi/Pt mol. ratio[a]	Pt crystallite size[b] (nm)
$Pt_{3.7}$/C	–	4
$Bi_{0.9}Pt_{3.5}$/C	0.24	4
$Bi_{2.2}Pt_{3.5}$/C	0.59	6
$Bi_{3.7}Pt_{3.5}$/C	0.98	8
$Pt_{3.7}/ZrO_2$	–	7
$Bi_{0.9}Pt_{3.5}/ZrO_2$	0.24	5

[a] Measured by ICP-OES.
[b] Calculated by XRD.

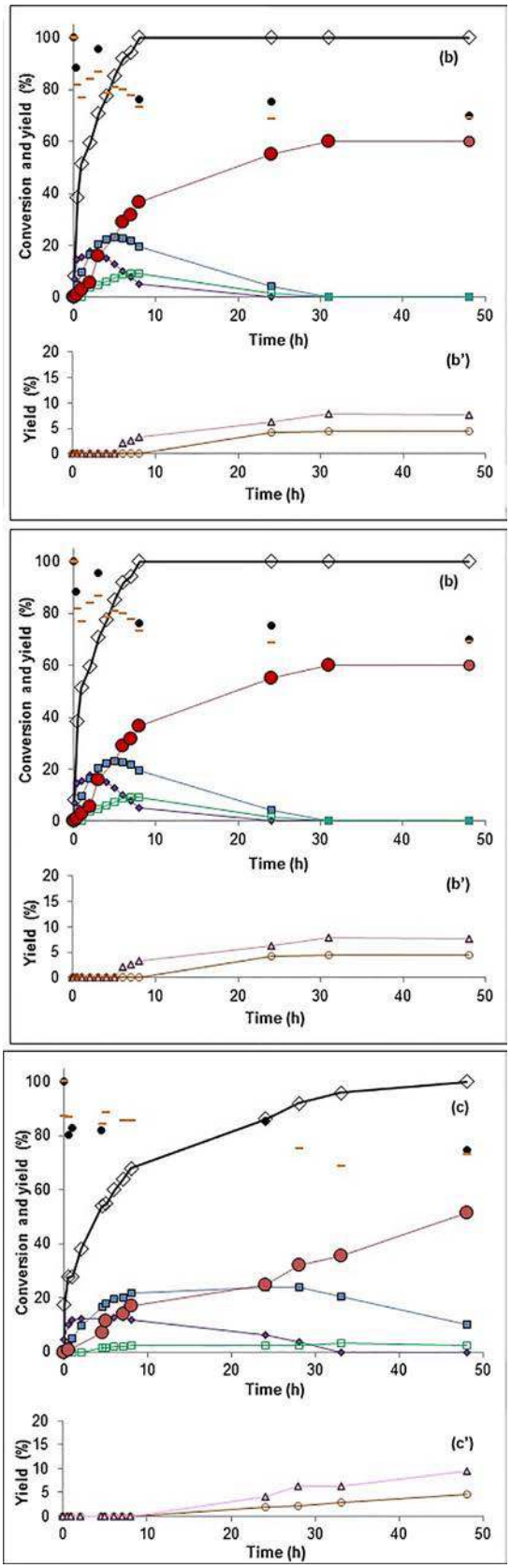

Fig. 1. Oxidation of 1,6-hexanediol (HDO) in water over (a and a') $Pt_{3.7}$/C, (b and b') $Bi_{0.9}Pt_{3.5}$/C (Bi/Pt = 0.24), and (c and c') $Bi_{2.2}Pt_{3.5}$/C (Bi/Pt = 0.59). (◇) Conversion, yields of (●) 6-hydroxyhexanal, ALD, (■) 6-hydroxyhexanoic acid, HA, (□) 6-oxohexanoic acid, AA, (●) adipic acid, DA, (○) glutaric acid, GLU, and (▲) succinic acid, SUC, and (▬) carbon balance, (●) TOC. Reaction conditions: 0.1 M HDO, HDO/Pt molar ratio = 100, 70 °C, and 40 bar of air.

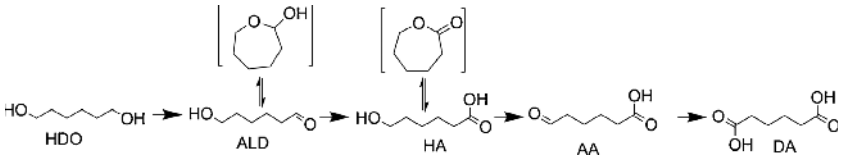

Scheme 1. Sequential oxidation of 1,6-hexanediol to adipic acid over Pt/C catalyst.

oxidation of 1,6-hexanediol (HDO) at 70 °C under 40 bar of air (substrate/Pt = 100). Fig. 1 shows the evolution of the reaction as a function of time over $Pt_{3.7}$/C (Fig. 1a), $Bi_{0.9}$-$Pt_{3.5}$/C (Bi/Pt = 0.24, Fig. 1b), and $Bi_{2.2}Pt_{3.5}$/C (Bi/Pt = 0.59, Fig. 1c). The conversion of HDO, the yields of the different intermediates and of adipic acid (DA), carbon balance, and TOC are included Fig. 1.

Over $Pt_{3.7}$/C, HDO conversion was ca. 25% at time zero; however, no product other than HDO was detected by HPLC analysis, in agreement with TOC measured. This observation suggests strong adsorption of either HDO or the first partially oxidized products on the catalyst surface. Then, conversion of HDO under air was rapid and it was complete within 4 h of reaction. The intermediates detected were 6-hydroxyhexanal (ALD), 6-hydroxyhexanoic acid (or 6-hydroxycaproic acid, HA), 6-oxohexanoic acid (AA) and adipic acid (DA). The main product at the beginning of the reaction was ALD, followed by the formation of HA, AA, and DA. The profiles of concentrations of the different products indicate that adipic acid was formed by sequential oxidation of 1,6-hexanediol as shown in Scheme Scheme 1. The diol is oxidized to the hydroxyaldehyde (ALD) and then to the hydroxyacid (HA). HA is further oxidized at the second alcohol function to the oxoacid (AA) and to the diacid (DA) product. Oxidation of the second alcohol group in HA was clearly less rapid than the oxidation of the first alcohol group in HDO. This general reaction pathway was also observed during oxidation of HDO in 0.35 M acetic acid aqueous solution over Pt/C [44]. As mentioned in the experimental part, neither the cyclic lactol nor ε-caprolactone were observed, because of the rapid interconversion with the open chains that were rapidly oxidized in water. Adipic acid was the major product after 3 h. The yield of adipic acid increased over time as the different intermediates were oxidized to reach a final yield of ca. 60%.

Results also indicated that degradation of the C6 oxygenated compounds occurred. Indeed, after about 3 h reaction time (HDO conversion above 95%), glutaric acid (GLU) and succinic acid (SUC) were identified as secondary products (Fig. 1a', b', c') besides the expected products; their concentration increased to attain yields of GLU and SUC at 3.8% and 5.1%, respectively. The final product DA was stable and did not undergo subsequent oxidative degradation, suggesting that the partially oxidized products were the precursors to the lower diacids GLU and SUC. The decarbonylation of an aldehyde function of ALD and AA to CO that subsequently can be oxidized to produce CO_2 could be a possible pathway [44].

The carbon balance from HPLC analysis and the TOC data in liquid phase matched relatively well as a function of time, thus confirming the strong adsorption of the substrate or intermediates from the start of the reaction, and the occurrence of consecutive reactions contributing to the formation of GLU and SUC.

The profile of the reaction over the Bi-modified $Bi_{0.9}$-$Pt_{3.5}$/C catalyst (Bi/Pt = 0.24; Fig. 1b–b') was not significantly different, albeit the reaction rates of oxidation of HDO and of intermediates were lowered. Indeed, complete conversion of HDO and the intermediates to DA was obtained before ca. 30 h of reaction vs. 22 h over $Pt_{3.7}$/C. The final yield of adipic acid was 61%, similar to that over Pt/C. GLU and SUC were also formed on the Bi-modified catalyst and the yields after 48 h were of 4.4% and 7.7%, respectively. A relatively fair agreement was also observed between the carbon balance and TOC; however, a significant gap compared to the initial TOC was still noticed, which confirms adsorption of products on the solid.

The addition of higher amounts of Bi over $Pt_{3.7}$/C on the catalytic performance is further illustrated in Fig. 1c–c' for $Bi_{2.2}$-$Pt_{3.5}$/C (Bi/Pt = 0.59). The reaction rate of oxidation for the first primary alcohol group (which yields ALD) was much lower. Indeed, the time of reaction to achieve total conversion of HDO increased from 4 h, for $Pt_{3.7}$/C, to 8 h and 48 h for $Bi_{0.9}$-$Pt_{3.5}$/C (Bi/Pt = 0.24) and $Bi_{2.2}$-$Pt_{3.5}$/C (Bi/Pt = 0.59), respectively. GLU and SUC were observed as by-products. At a still higher Bi/Pt molar ratio of 0.98 ($Bi_{3.7}Pt_{3.5}$/C, not shown), HDO conversion was only 65% after 48 h.

To summarize, the addition of Bi had a detrimental effect on the reaction rate at Bi/Pt > 0.6, hence on the final DA yield. The results may be discussed in relation to those of Davis et al, who also compared Pt/C and Bi-promoted Pt/C in the oxidation of HDO (0.1 M aqueous solutions) [43,44]. The impact of adding Bi to Pt depended on the O_2 pressure. In the range of 0.2–2 bar O_2, different reaction orders with respect to O_2 were obtained for Pt/C (order of 0.75) and Bi-Pt/C (order close to zero), which accounted for the significant promotion effect of Bi on the reaction rate under low O_2 pressures. Under higher O_2 pressures (2–10 bar), the promotional effect of Bi was no more observed, and Bi-Pt/C became even less active. The present results (Fig. 2) are in agreement with the literature, as no promotional effect of Bi was observed under partial pressure of 8 bar of O_2 (40 bar of air).

More generally, the reaction profiles of oxidation of HDO over the Bi-promoted catalysts supported on active carbon were relatively the same as over $Pt_{3.7}$/C (Fig. 1). However, the Bi-Pt catalysts displayed a lowered rate for the oxidation of primary alcohol functions, either of HDO to ALD, or of HA to AA. Conversely, once formed, the oxo functional groups in the intermediates were rapidly converted to the carboxylic groups and yielded HA and DA. Finally, no improvement in the final yield of DA was noted compared with the $Pt_{3.7}$/C catalyst (yield of ca. 60%). The TOC and carbon balance showed the same trends as for $Pt_{3.7}$/C: a satisfying carbon balance, but a strong adsorption of HDO and the first intermediates on the catalyst. Over all the carbon supported Pt catalysts, GLU and SUC were observed as by-products.

The influence of the nature of the support was examined by using ZrO_2 as the support. The XRD patterns are shown in Fig. S1, and Table 1 summarizes the mean size of Pt crystallites, which are similar to the ones on active carbon. Fig. 2 displays the reaction profiles over $Pt_{3.7}$/ZrO_2 and $Bi_{0.9}Pt_{3.5}$/ZrO_2 (Bi/Pt = 0.24).

Over both catalysts, the carbon balance and the TOC values were close, however, some loss of carbon in the aqueous phase in the form of adsorbed compounds or as gaseous products in the headspace of the reactor was evidenced. Comparison under identical conditions of carbon and zirconia- supported monometallic (Figs. 1a and Figure 2a) and Bi-modified catalysts (Fig. 1b and Fig. 2b, respectively) shows that the reaction rate of HDO conversion was slightly faster using ZrO_2 as the support; total conversion of HDO was achieved within 2 h over $Pt_{3.7}$/ZrO_2 (Fig. 2a) vs. 3 h over $Pt_{3.7}$/C (Fig. 1a), and within 3 h over $Pt_{0.9}$-$Bi_{3.5}$/ZrO_2 (Fig. 2b) vs. 5 h over $Pt_{0.9}$-$Bi_{3.5}$/C (Fig. 1b). In contrast, the oxidation rates of the formed reaction intermediates were significantly slowed down over ZrO_2 (Figs. 1 and 2). The maxima of ALD (formed after oxidation of one primary alcohol) and AA (oxidation of second CH_2OH function) concentrations were higher than over the carbon support. Therefore, the oxidation of the aldehyde groups to the carboxylic ones were slower over the zirconia support.

Interestingly, glutaric and succinic acid were not detected over the ZrO_2-supported catalysts, which suggests that the carbon support microporosity might be responsible for their formation. It was suggested in the literature that the presence of oxygen-function groups on a

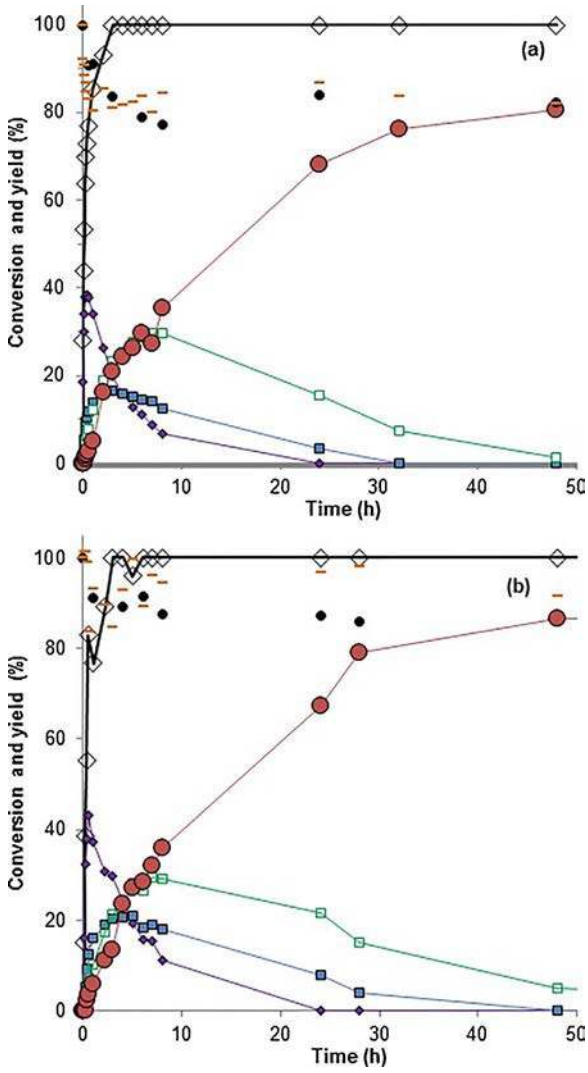

Fig. 2. Oxidation of 1,6-hexanediol (HDO) over (a) $Pt_{3.7}/ZrO_2$ and (b) $Bi_{0.9}Pt_{3.5}/ZrO_2$ (Bi/Pt = 0.24). (◇) Conversion, (●) 6-hydroxyhexanal, ALD, (■) 6-hydroxyhexanoic acid, HA, (□) 6-oxohexanoic acid, AA, (●) adipic acid, DA, and (▬) carbon balance, (●) TOC. Reaction conditions: 0.1 M HDO, HDO/Pt molar ratio = 100, 70 °C, 40 bar air.

carbon support may promote the hydrophilicity, and thus the adsorption of water or oxygenated compounds, and the conversion of adipic acid to glutaric and succinic acid over a Pt/C under air pressure [59]. In the present study, the support was not pre-oxidized before Pt deposition, so that this effect may be ruled out. Despite the fact that the reaction proceeded at a lower rate for intermediates up to DA over the ZrO_2 supported catalyst, the final yield of DA reached 80%. The absence of by-products may have contributed to this higher yield.

Fig. 3 summarizes the influence of the addition of different amounts of Bi on the final yields at 48 h for the series of C and ZrO_2-supported catalysts. No positive effect of the promotion by Bi was noted.

Finally, ICP-OES analysis of the final reaction media revealed significant leaching of Pt-Bi bimetallic systems: approximately 13% of leaching of Bi was detected in the final reaction medium using Bi-Pt/C (Bi/Pt = 0.24), that is a weakness for their potential multiple reuse. Leaching of Pt was less than 2% of the loaded metal.

3.2. Bimetallic Au-Pt/ZrO_2 and Au-Pd/ZrO_2 catalysts

The series of bimetallic Au-Pt and Au-Pd catalysts were prepared on ZrO_2 support to avoid formation of by-products (vide supra). The Au/Pt or Au/Pd molar ratios were chosen in a large range to detect an optimal

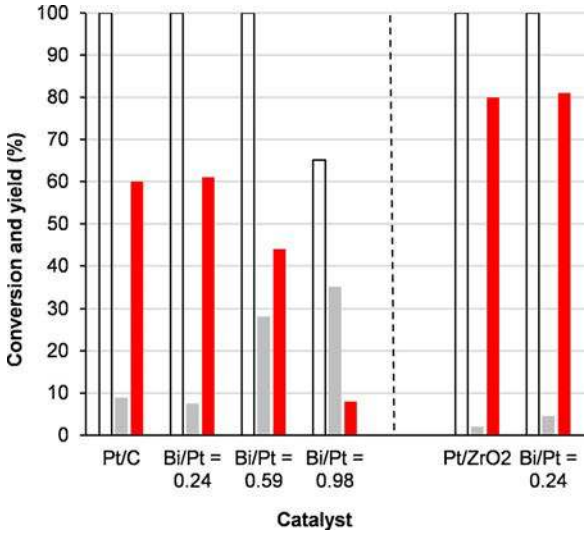

Fig. 3. Conversion and yields of products at 48 h over the Pt and Bi-Pt catalysts supported on C (left) or ZrO_2 (right). Reaction conditions: 0.1 M HDO, HDO/Pt molar ratio = 100, 70 °C, 40 bar air. (□) HDO conversion, (■) yield of DA, (▬) yield of partially oxidized products plus by-products.

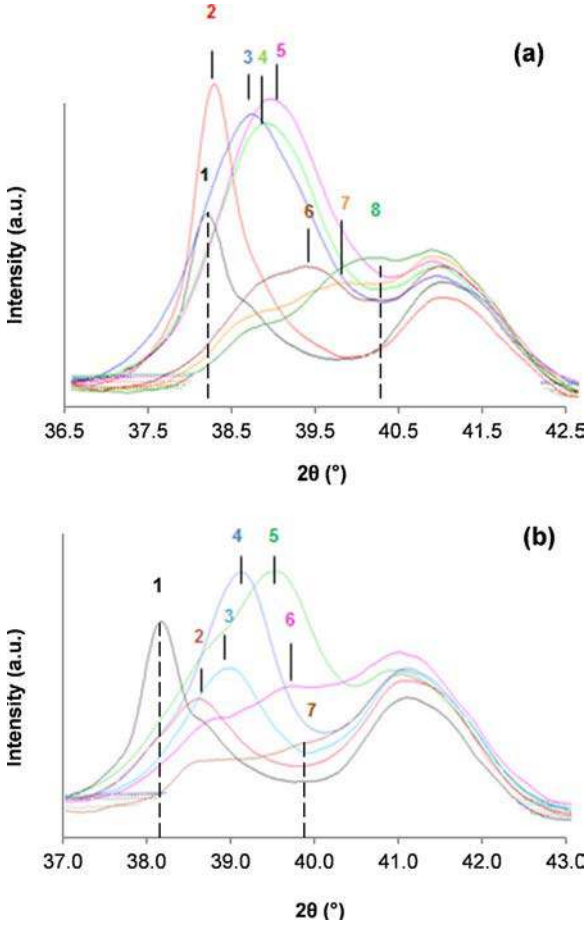

Fig. 4. Powder XRD patterns of zirconia supported (a) Au, Au-Pt, and Pt catalysts, and (b) Au, AuPd, and Pd catalysts. (1) $Au_{3.6}/ZrO_2$, (2) $Au_{3.9}Pt_{0.6}/ZrO_2$ (6.4), (3) $Au_{5.2}Pt_{3.1}/ZrO_2$ (1.66), (4) $Au_{3.0}Pt_{3.3}/ZrO_2$ (0.9), (5) $Au_{2.8}Pt_{3.6}/ZrO_2$ (0.77), (6) $Au_{1.4}Pt_{3.3}/ZrO_2$ (0.42), (7) $Au_{0.5}Pt_{3.1}/ZrO_2$ (0.16), (8) $Pt_{3.7}/ZrO_2$. (1) $Au_{3.6}/ZrO_2$ (1), $Au_{1.0}Pd_{3.5}ZrO_2$ (Au/Pd = 4.14), (3) $Au_{2.1}Pd_{1.0}/ZrO_2$ (Au/Pd = 1.13), (4) $Au_{2.5}Pd_{1.6}/ZrO_2$ (Au/Pd = 0.84), (5) $Au_{4.0}Pd_{3.8}/ZrO_2$ (0.57), (6) $Au_{1.0}Pd_{3.5}/ZrO_2$ (0.15), (7) $Pd_{3.1}/ZrO_2$. The dashed lines represent the expected positions for the (111) peaks of Au, Pt, and Pd.

Table 2
Composition, particle size of ZrO_2 supported Pt, Au, Pd, Au-Pt, and Au-Pd catalysts.

Catalyst	Au/Pt[a] or Au/Pd[a]	Metal load[a] (%)	Crystallite size[b] (nm)
$Pt_{3.7}/ZrO_2$	–	3.7	7
$Au_{0.5}Pt_{3.1}/ZrO_2$	0.16	3.6	5
$Au_{1.4}Pt_{3.3}/ZrO_2$	0.42	4.7	5
$Au_{2.8}Pt_{3.6}/ZrO_2$	0.77	6.4	5
$Au_{3.0}Pt_{3.3}/ZrO_2$	0.90	6.3	5
$Au_{5.2}Pt_{3.1}/ZrO_2$	1.66	8.3	5
$Au_{3.9}Pt_{0.6}/ZrO_2$	6.40	4.5	9
$Au_{3.6}/ZrO_2$	–	3.6	11
$Au_{1.0}Pd_{3.5}/ZrO_2$	0.15	4.5	3
$Au_{4.0}Pd_{3.8}/ZrO_2$	0.57	7.8	5
$Au_{2.5}Pd_{1.6}/ZrO_2$	0.84	4.1	9
$Au_{2.1}Pd_{1.0}/ZrO_2$	1.13	3.1	6
$Au_{2.3}Pd_{0.3}/ZrO_2$	4.14	2.6	4
$Pd_{3.1}/ZrO_2$	–	3.1	6

[a] Measured by ICP-OES.
[b] Of the alloy, as calculated by XRD.

composition. Fig. 4 shows the XRD patterns of the Au, Pt, Pd, Au-Pt, and Au-Pd catalysts in the 2θ ranges between 36.5 and 43° typical of (111) reflections of Au, Pt and Pd. Table 2 summarizes the actual loadings of the catalysts, which were relatively close to the nominal loadings, and the mean crystallite size measured for the metals.

Au and Pd or Pt can form solid solutions over the whole range of atomic ratios. Bimetallic nanoparticles can generate different configurations (e.g. core-shell, alloy) [63]. Nevertheless, the preparation of supported bimetallic Au-Pt or Au-Pd by co-wet impregnation and reduction with $NaBH_4$ usually leads to the formation of alloy [62,64]. Notably, the XRD patterns of all bimetallic catalysts clearly revealed the presence of the main (111) peak line which lies between the diffraction line of pure Au (2θ = 38.2°) and Pt (2θ = 39.8°), or Pd (2θ = 40.2°) monophases (Fig. 4). In all samples, only a single alloy structure was observed and no other diffraction peak corresponding to Au or Pt (or Pd) was recognized. This indicates the successful formation of Au-Pt and Au-Pd alloys. The shift of the diffraction peak decreased to lower diffraction angles with increasing Au content in the bimetallic systems (Fig. 4). The lattice parameters of Pt, Pd, and Au are 3.92 Å, 3.89 Å, and 4.07 Å, respectively; the lattice parameters of the different bimetallic catalysts were estimated from the XRD diffraction pattern. They are plotted in Fig. S2 as a function of the Au amount in Au-Pd and Au-Pt catalysts. This figure also represents the linear relation obtained by applying Vegard's law to the Au-Pd and Au-Pt bimetallic systems. Increasing the concentration of Au led to an increase in the experimentally determined lattice distance with no significant deviation from Vegard's law, which indicates the presence of alloying [53,65,66].

The morphology of the Au-Pt and Au-Pd bimetallic nanoparticles were further characterized by TEM. Some representative recorded pictures of the supported Au-Pt (Au/Pt = 0.77) and Au-Pd (Au/Pd = 0.84) catalysts are shown in Fig. 5.

As shown previously for similar Au-Pt catalysts supported on TiO_2 or ZrO_2 using the same method of preparation [64], both Au-Pt and Au-Pd catalysts showed individual bimetallic nanoparticles and agglomerates forming nanochains of two or several nanoparticles of average size in the range from 5–10 nm, in agreement with XRD results. EDX spectra acquired on different zones containing several metallic particles showed that both Au and Pt or Pd are present within the nanoparticles (Fig. 5a3 and b2). The relative Au/Pt or Au/Pd ratios determined by EDX (0.63 and 0.82, respectively) were relatively close to the nominal composition resulting from ICP-OES analysis (0.77 and 0.84, respectively), strongly supporting the formation of single-phase alloys.

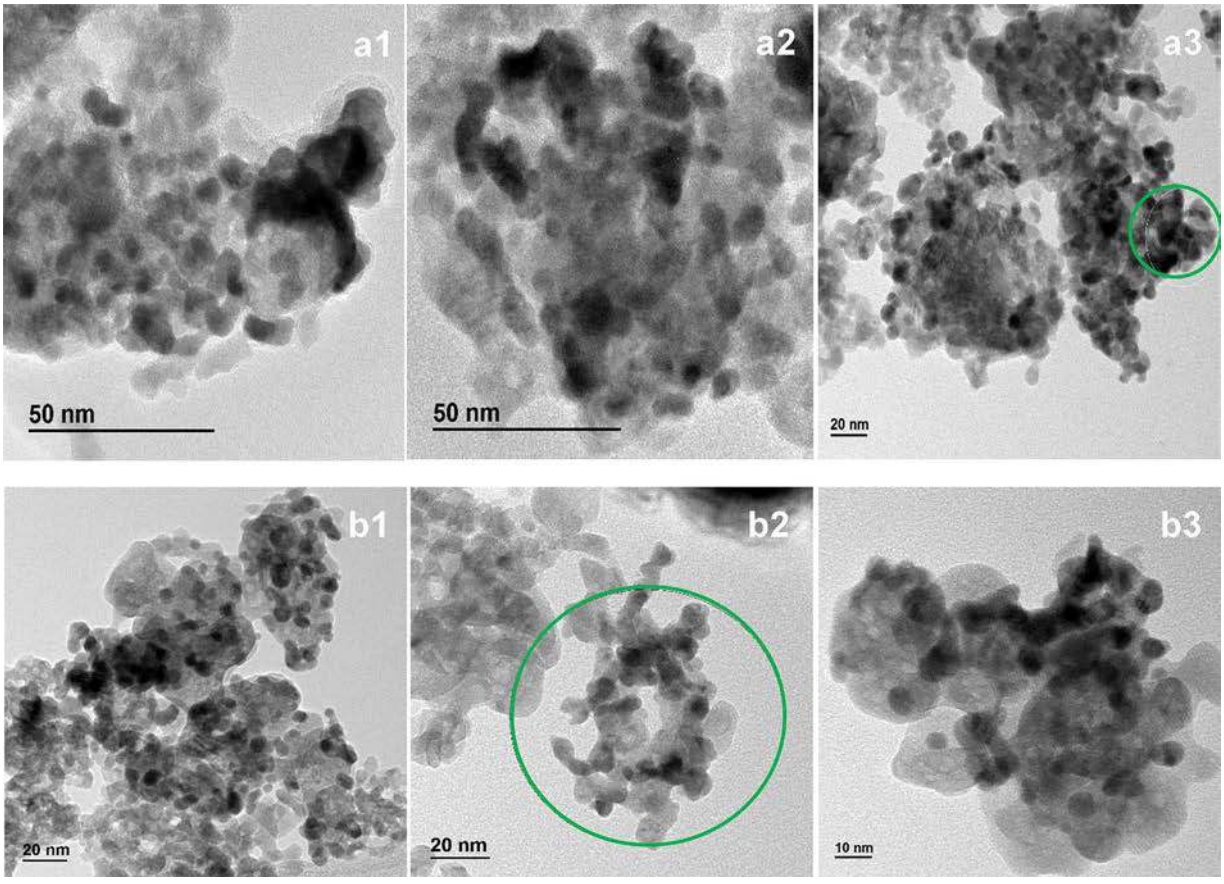

Fig. 5. Representative TEM images of (a) Au-Pt (Au/Pt = 0.77) and (b) Au-Pd (Au/Pd = 0.84) catalysts; the EDX analysis display Au/Pd atomic ratios of 0.63 (Fig. a3) and 0.82 (Fig. b2), respectively.

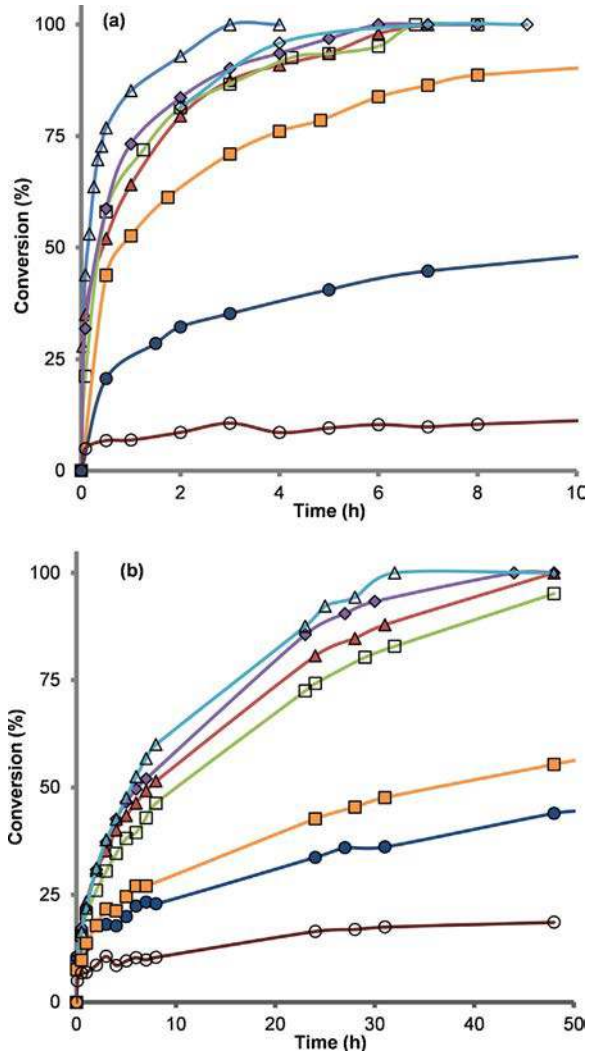

Fig. 6. HDO conversion as a function of time over supported- (a) Au, Au-Pt, and Pt catalysts: (O) $Au_{3.6}/ZrO_2$, (●) $Au_{3.9}Pt_{0.6}/ZrO_2$ (Au/Pt = 6.4), (■) $Au_{5.2}Pt_{3.1}/ZrO_2$ (Au/Pt = 1.66), (◆) $Au_{3.0}Pt_{3.3}/ZrO_2$ (Au/Pt = 0.9), (◊) $Au_{2.8}Pt_{3.6}/ZrO_2$ (Au/Pt = 0.77), (□) $Au_{1.4}Pt_{3.3}/ZrO_2$ (Au/Pt = 0.42), (▲) $Au_{0.5}Pt_{3.1}/ZrO_2$ (Au/Pt = 0.16), (△) $Pt_{3.7}/ZrO_2$, and (b) Au, Au-Pd, and Pd catalysts: (O) $Au_{3.6}/ZrO_2$, (●) $Pd_{3.1}/ZrO_2$, (■) $Au_{2.3}Pd_{0.3}/ZrO_2$ (Au/Pd = 4.14), (□) $Au_{4.0}Pd_{3.8}/ZrO_2$ (Au/Pd = 0.57), (▲) $Au_{1.0}Pd_{3.5}/ZrO_2$ (Au/Pd = 0.15), (◆) $Au_{2.5}Pd_{1.6}/ZrO_2$ (Au/Pd = 0.84), (△) $Au_{2.1}Pd_{1.0}/ZrO_2$ (Au/Pd = 1.13). Reaction conditions: HDO (0.1 M), HDO/metal = 100, 70 °C, 40 bar of air.

Fig. 6a and b compare the profiles of HDO conversion as a function of time over the series of Au-Pt/ZrO_2 and Au-Pd/ZrO_2 catalysts, respectively.

The catalytic activity was significantly affected by the composition. First, the monometallic catalysts exhibited very different reaction rates. $Pt_{3.7}/ZrO_2$ was fairly active (conversion was complete after 3 h), whereas $Pd_{3.1}/ZrO_2$ (44% conversion after 48 h) and $Au_{3.6}/ZrO_2$ (only 17% conversion after 48 h) were comparatively very poorly active. The higher activity for Pt catalyst is in line with its known activity for alcohol oxidation in neutral medium, as described for several alcohols such as glycerol, glyoxal and methanol [67]. In contrast, Au catalysts, and to some extent Pd catalysts, usually show very low or no activity in non-alkaline medium [68].

Upon addition of a small amount of Au to Pt and formation of an alloy, the reaction rate of HDO conversion was sensitively lower than over Pt. For instance, the time to attain 80% conversion was only 0.6 h over Pt vs. 2 h over $Au_{0.5}Pt_{3.1}/ZrO_2$ (Au/Pt = 0.14). Higher Au/Pt molar ratio (up to 0.9) did not influence significantly the rate of reaction and total conversion of HDO was attained within 6–7 h of reaction.

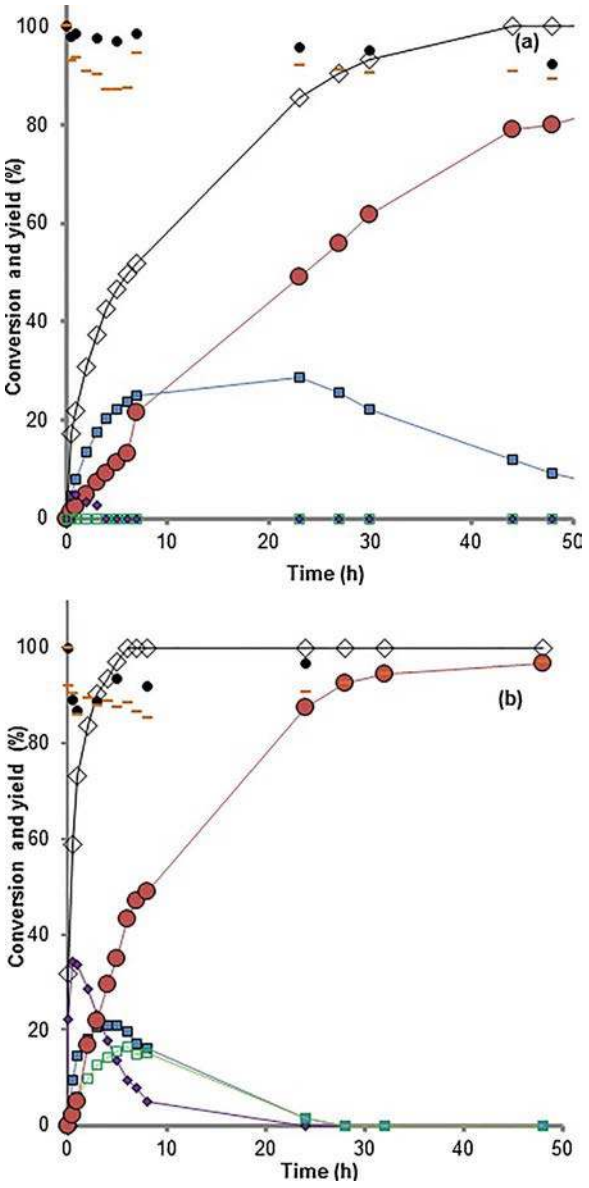

Fig. 7. HDO conversion and yields of products over (a) $Au_{2.5}Pd_{1.6}/ZrO_2$ (Au/Pd = 0.84) and (b) $Au_{2.8}Pt_{3.6}/ZrO_2$ (Au/Pt = 0.77). Reaction conditions: HDO (0.1 M), HDO/metal = 100, 70 °C, 40 bar of air. (◇) Conversion, (●) 6-hydroxyhexanal, ALD, (■) 6-hydroxyhexanoic acid, HA, (□) 6-oxohexanoic acid, AA, (●) adipic acid, DA, and (–) carbon balance, (●) TOC.

The activity then dropped drastically for Au/Pt ratio of 1.66 and HDO conversion was even not complete after 48 h for Au/Pt = 6.4.

The opposite trend was observed for activity with addition of Au to Pd vs. Pt. The Pd catalyst was little active for oxidation of HDO. The formation of the alloy significantly improved the reaction rate of HDO conversion (Fig. 6b). However, the Au-Pd catalysts remained much less active than the Au-Pt catalysts under the same reaction conditions (Fig. 6a and b).

Fig. 7 shows the reaction profiles as a function of time over a Au-Pd catalyst, namely $Au_{2.5}Pd_{1.6}ZrO_2$ (Fig.7a, Au/Pd = 0.84), and over a Au-Pt catalyst, namely catalyst $Au_{2.8}Pt_{3.6}/ZrO_2$ (Fig. 7b, Au/Pt = 0.77). Fig. 8 illustrates HDO conversion and yields of intermediates and by-products at 48 h of reaction for the monometallic catalysts and the series of Pt-Au/ZrO_2 and Pd-Au/ZrO_2 bimetallic catalysts.

Over Au-Pd/ZrO_2, the oxidation reactions of the aldehyde groups to the acids were so rapid that the maximum yields of ALD (5%) and AA (nul) were very low (Fig. 7a). These observations show that the relative

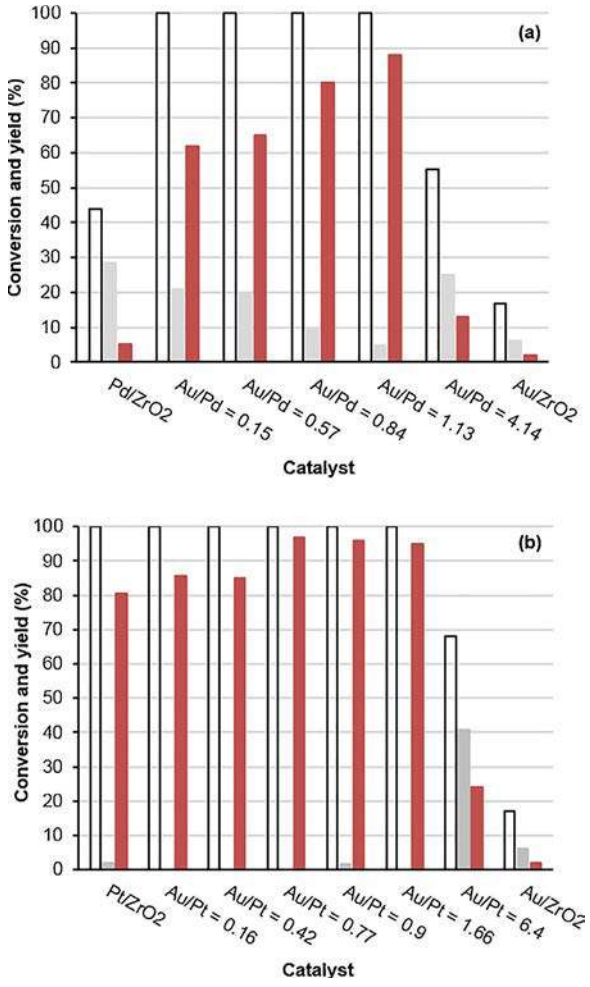

Fig. 8. Effect of catalyst composition on (□) HDO conversion, (■) yield of DA, and (■) yield of partially oxidized products (ALD, HA, AA) after 48 h reaction over mono and bimetallic catalysts under the reaction conditions: HDO (0.1 M), HDO/metal = 100, 70 °C, 40 bar of air.

rates of oxidation of the different functions (alcohol or aldehyde) were different. Conversion of the intermediates, predominantly HA, was not complete after 48 h of reaction. The maximum yield of DA of 80–88% after 48 h was observed for catalysts containing a Au/Pd ratio of ca.1 (Fig. 8a) which were also the most active. The reaction was slow over Au-Pd, however, when the reaction was allowed to continue for 120 h, the final yield attained 95% and all intermediates were converted (not shown). Moreover, an increase of the temperature from 70 °C to 90 °C resulted in a final DA yield of 96% after 30 h over $Au_{2.5}Pd_{1.6}/ZrO_2$ (Au/Pd = 0.84), (not shown).

Over $AuPt/ZrO_2$, HDO was rapidly converted (within 8 h) and the rate of conversion of the intermediates was slower (Fig. 7b). A similar pathway upon conversion of HDO was observed as the one presented previously over Pt catalysts and thus, regardless of the second metal (Bi, Au), and of the support: sequential oxidation reactions occurs from the diol to the diacid product with a final yield of 97%. Over all Pt catalysts the rate of oxidation of HDO was much faster than the one of HA oxidation. Despite the six carbon length of the molecule, the proximity of a COOH group lowered the further oxidation of the second primary alcohol. No significant concentrations of AA were observed, therefore, the oxidation of the aldehyde function of AA is not the limiting step. The yield of DA after 48 h increased progressively from 80% over the Pt catalyst to a wide maximum of 95–97% for Au/Pt molar ratio range 0.77–1.66 and decreased rapidly to 24% after 48 h upon further addition of Au (Au/Pt = 6.4), since reaction was then too slow and 40% of partially oxidized intermediates were still present (Fig. 8b). Taking also into consideration the reaction rates (Fig. 6a), the best compromise seems to be a Au/Pt ratio of ca. 1.

Moreover, neither GLU nor SUC were formed over the ZrO_2-supported bimetallic Au-Pt and Au-Pd catalysts, the carbon balance and TOC values were always above 90%.

In summary, Au-Pd (Fig. 8a) and Au-Pt (Fig. 8b) bimetallic catalysts with a metal molar ratio around 1 allowed to achieve the best yield of diacid (Fig. 8). It is worth to note that Au-Pd catalysts could efficiently catalyze the oxidation reaction of HDO in water to completion in the absence of any soluble base, as usually required. For instance, active carbon or titania-supported Au-Pd alloyed nanoparticles showed better performances for oxidation of glycerol to glycerate or HMF to furandicarboxylate, however a base promoter was employed in the systems [53,69–71]. The high conversions which were sometimes claimed under base-free conditions for Au or Au-Pd catalysts supported on basic supports (hydrotalcite, MgO) were likely due to the extensive leaching of magnesium from the support and formation of $Mg(OH)_2$ acting as the soluble base [48,72]. Selective oxidation of conjugated alcohols (benzyl alcohol, crotyl alcohol, cinnamyl alcohol) to the aldehydes was possible in aqueous solution in the absence of base additives using Au-Pd core-shell nanoparticles [73]. A recent report suggests that bimetallic Au-Pd nanoparticles supported on carbon nanotubes may obviate this requirement of an excess amount of a soluble base for 5-HMF oxidation to FDCA [74]. The better activity of Au-Pd and Au-Pt compared with the monometallic counterparts for oxidation of butanediols in base-free aqueous media was attributed to the presence of alloys [75]. In the present work, the Au-Pt catalysts supported on zirconia were the most active under these conditions (70 °C, 40 bar of air, water). The yields of adipic acid observed (96%) are among the best ones described in the literature.

To gain more insight into the role of the metals on the reactions, Fig. 9 records the evolution of selectivity to each intermediate and to the diacid as a function of HDO conversion at 70 °C under 40 bar air over catalysts with different composition.

It shows that the distribution of products across the conversion of HDO depends strongly on the catalyst composition. At low conversion, the initial selectivity to 6-hydroxyhexanal (ALD) is high over the platinum-based catalysts and the oxidation of the aldehyde group of this intermediate takes place smoothly (Fig. 9a–c). A high selectivity to ALD at 90% HDO conversion over a Pt/C catalyst was observed during oxidation of α,ω- diols to diacids at acidic conditions [16]. On the contrary, in the presence of $Au_{2.5}Pd_{1.6}/ZrO_2$, this intermediate is very rapidly converted to 6-hydroxyhexanoic acid (HA), which is consequently formed with a high initial selectivity (Fig. 9d). Similarly, over this Au-Pd catalyst the oxidation of the aldehyde group of the subsequent intermediate oxohexanoic acid AA is very rapid so that it was almost not detected. It is clear that $Au\text{-}Pd/ZrO_2$ catalysts are very active for the oxidation of the aldehyde functions, which affects the reaction profiles of HDO oxidation over Au-Pd vs. Pt-based catalysts. In the latter cases, selectivity to adipic acid becomes significant only at high diol conversion.

3.3. Catalyst recyclability

To investigate the stability of the catalysts, recycling experiments were performed over $Au_{2.8}Pt_{3.6}/ZrO_2$ (Au/Pt = 0.77) catalyst. The sample was used for 6 successive reactions and the corresponding results are displayed in Fig. 10. No significant loss of catalytic activity was observed. The yield of DA after 48 h was still > 86% in the 6th experiment and the reaction mixture contained a few percent of HA and AA remaining to be converted. Moreover, no Au or Pt was detected in the post-reaction solution by ICP-OES analysis, indicating high chemical stability of the catalyst.

Furthermore, comparison of the diffraction patterns of different used catalysts and of the fresh ones indicates that the alloy phase was

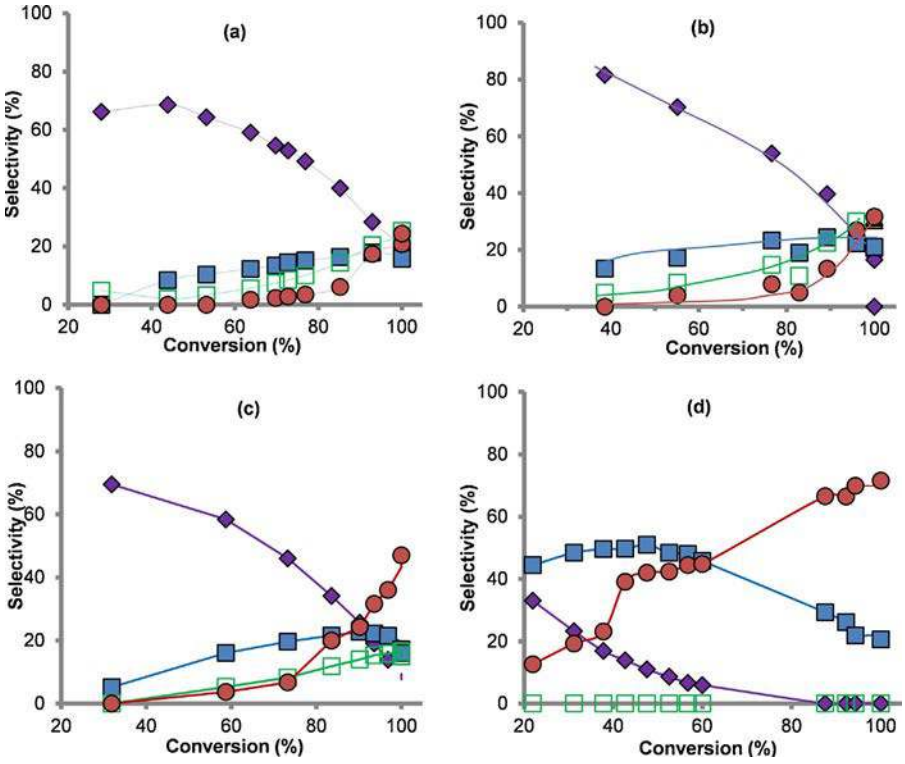

Fig. 9. Evolution of the selectivity to (●) ALD, (■) HA, (□) AA, and (●) DA as a function of HDO conversion over (a) Pt/ZrO_2, (b) $Bi_{0.9}Pt_{3.5}/ZrO_2$, (c) $Au_{2.8}Pt_{3.6}/ZrO_2$ and (d) $Au_{2.5}Pd_{1.6}/ZrO_2$ at 70 °C under 40 bar of air.

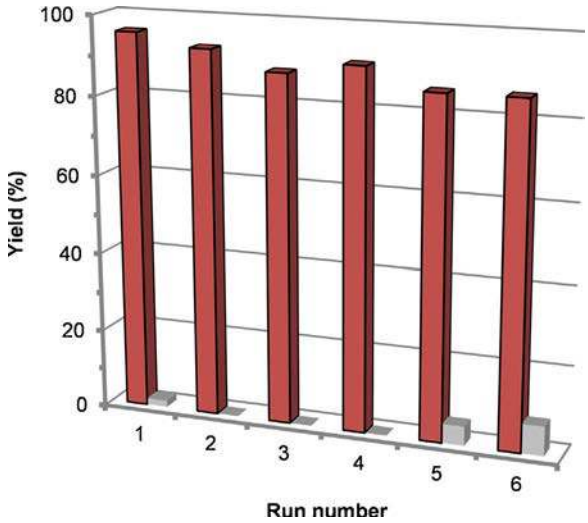

Fig. 10. Recyclability of $Au_{2.8}Pt_{3.6}/ZrO_2$ (Au/Pt = 0.77) in the oxidation of 1,6-HDO to adipic acid. Reaction conditions: HDO (0.1 M), HDO/metal = 100, 70 °C, 40 bar of air. (■) yield of DA, (■) yield of partially oxidized products (HA, AA).

not modified, in particular in the 2θ range 37–43°, and the mean crystallite size of the alloys remained constant at 5 nm (Figs. S3 and S4).

4. Conclusions

The aerobic oxidation of 1,6-hexanediol to adipic acid in water was examined under base-free conditions over supported Pt, Bi-Pt, Pd, Au, Au-Pd and Au-Pt nanoparticles. The reaction of HDO went through sequential oxidation reactions; first one alcohol function is oxidized to the acid via the aldehyde, then the second one. Bimetallic Au-Pd and Au-Pt catalysts on zirconia are highly effective. The Au-Pt catalysts have been shown to have higher catalytic activity than Au-Pd. The highest yields of 96% of the desired dicarboxylic acid was reached for the catalysts having a Au/Pd or Au/Pt atomic ratio of ca. 1. Furthermore, the Au-Pt catalyst showed good stability and maintained a high performance over 6 runs. To our knowledge, this is one of the best result in the absence of base for aerobic oxidation of 1,6-hexanediol, which opens a route to sustainable oxidation of this family of substrates.

Acknowledgements

This work was financially supported by the Agence Nationale de la Recherche (ANR) within the French-Luxembourg program under Award Number ANR-15-CE07-0017-02, ANR Catbiose. The authors gratefully acknowledge Denilson Da Silva Perez (FCBA, France) and Youssef Habibi (LIST, Luxembourg) for fruitful discussions.

Appendix A. Supplementary data

Supplementary material related to this article can be found, in the online version, at doi:https://doi.org/10.1016/j.apcata.2017.12.005

References

[1] P. Oppenheim, G.L. Dickerson, Kirk-othmer encyclopedia of chemical technology, 5th edition, Adipic Acid 1 John Wiley & Sons, 2004, pp. 553–582.
[2] S.V. de Vyver, Y. Roman-Leshkov, Catal.. Sci. Technol. 3 (2013) 1465–1479.
[3] R. Beerthuis, G. Rothenberg, N.R. Shiju, Green Chem. 17 (2015) 1341–1361.
[4] Adipic Acid Market Analysis By Application (Nylon 6,6 Fiber, Nylon 6,6 Resin, Polyurethane, Adipate Ester) And Segment Forecasts To 2020, Published: February 2014, 90 Pages, Report ID: 978-1-68038-078-1.
[5] T.N. Smith, K.R. Hash, Carbohydr. Res. 350 (2012) 6–13.
[6] B.G. Hermann, K. Blok, M.K. Patel, Environ. Sci. Technol. 41 (2007) 7915–7921.
[7] K. Sato, M. Aoki, R. Noyori, Science 281 (1998) 1646–1647.
[8] R. Noyori, M. Aoki, K. Sato, Chem. Commun.. (2003) 1977–1986.
[9] S. Ghosh, S.S. Acharyya, S. Adak, L.S. Konathala, T. Sasaki, R. Bal, Green Chem. 16 (2014) 2826–2834.
[10] L. Meng, S. Zhai, Z. Sun, F. Zhang, Z. Xiao, Q. An, Microporous Microporous Mater. 204 (2015) 123–130.
[11] J. Dai, W. Zhong, W. Yi, M. Liu, L. Mao, Q. Xu, D. Yin, Appl. Catal. B-Environ. 192 (2016) 325–341.
[12] R.F. Parton, I.F.J. Vankelecom, M.J.A. Casselman, C.P. Bezoukhanova, J.B. Uytterhoeven, P.A. Jacobs, Nature 370 (1994) 541–544.
[13] D. Bonnet, T. Ireland, E. Fache, J.-P. Simonato, Green. Chem. 8 (2006) 556–559.

[14] A. Alshammari, A. Koeckritz, V.N. Kalevaru, A. Bagabas, A. Martin, ChemCatChem 4 (2012) 1330–1336.
[15] M. Besson, F. Gauthard, B. Horvath, P. Gallezot, J. Phys. Chem. B 109 (2004) 2461–2467.
[16] F. Cavani, L. Ferroni, A. Frattini, C. Lucarelli, A. Mazzini, K. Raabova, S. Alini, P. Accorinti, P. Babini, Appl. Catal. A: Gen. 391 (2011) 118–124.
[17] A. Dutta, M. Pramanik, A.K. Patra, M. Nandi, H. Uyama, A. Bhaumik, Chem. Commun. 48 (2012) 6738–6740.
[18] Y. Usui, K. Sato, Green Chem. 5 (2003) 373–375.
[19] M. Moudjahed, L. Dermeche, S. Benadji, T. Mazari, C. Rabia, J. Mol. Catal. Chem. 414 (2016) 72–77.
[20] A. Castellan, J. Bart, S. Cavallaro, Catal. Today 9 (1991) 255–283.
[21] J. Han, Energy Convers. Manage. 129 (2016) 75–80.
[22] S. Gunukula, R.P. Anex, Biofuels Bioprod. Bioref. 11 (2017) 897–907.
[23] T.R. Boussie, E.L. Dias, Z.M. Fresco, V.J. Murphy, Production of adipic acid and derivatives from carbohydrate-containing materials. US Pat. 2010/0317822 (2010), to Rennovia.
[24] T.R. Boussie, E.L. Dias, Z.M. Fresco, V.J. Murphy, J. Shoemaker, R. Archer, H. Jiang, Production of Adipic Acid and Derivatives from Carbohydrate-Containing Materials, US Pat. 2014/8669397 (2014), to Rennovia.
[25] G.M. Diamond, V. Murphy, T.R. Boussie, A. Hagemeyer, A.F. Volpe Jr., Application of high throughput experimentation to the production of commodity chemicals from renewable feedstocks, Modern Applications of High Throughput R & D in Heterogeneous Catalysts, Bentham Science Publishers, 2014, pp. 288–309.
[26] P. Lanzafame, S. Perathoner, G. Centi, A vision for future biorefineries, in: F. Cavani, S. Albonetti, F. Basile, A. Gandini (Eds.), Chemicals and Fuels from Bio-Based Building Blocks, 1 Wiley VCH, 2016, pp. 497–518 Ch. 18.
[27] K.M. Draths, J.W. Frost, J. Am. Chem. Soc. 116 (1994) 399–400.
[28] W. Niu, K.M. Draths, J.W. Frost, Biotechnol. Prog. 18 (2002) 201–211.
[29] J.M. Thomas, R. Raja, B.F.G. Johnson, T.J. O'Connell, G. Sankar, T. Khimyak, Chem. Commun. 9 (2003) 1126–1127.
[30] D.R. Vardon, N.A. Rorrer, D. Salvachua, A.E. Settle, C.W. Johnson, M.J. Menart, N.S. Cleveland, P.N. Ciesielski, K.X. Steirer, J.R. Dorgan, G.T. Beckham, Green Chem. 18 (2016) 3397–3413.
[31] S. Scelfo, R. Pirone, N. Russo, Catal. Commun. 84 (2016) 98–102.
[32] J.G. DeVries, T. Buntara, P. Huat Phua I.V. Melian-Cabrera, H.J. Heeres, Preparation of caprolactone, caprolactam, 2,5-tetrahydrofuran-dimethanol, 1,6-hexanediol or 1,2,6-hexanetriol from 5-hydroxymethyl-2-furfuraldehyde, WO Pat. 2011/149339 (2011), to NWO.
[33] T. Buntara, S. Noel, P.H. Phua, I. Melián-Cabrera, J.G. de Vries, H.J. Heeres, Angew. Chem. Int. Ed. 50 (2011) 7083–7087.
[34] T. Buntara, S. Noel, P.H. Phua, I. Melián-Cabrera, J.G. Vries, H.J. Heeres, Top. Catal. 55 (2012) 612–661.
[35] R. Alamillo, M. Tucker, M. Chia, Y. Pagan-Torres, J. Dumesic, Green Chem. 14 (2012) 1413–1419.
[36] K. Chen, S. Koso, T. Kubota, Y. Nakagawa, K. Tomishige, ChemCatChem 2 (2010) 547–555.
[37] M. Chia, Y.J. Pagan-Torres, D. Hibbits, Q. Tan, H.N. Pham, A.K. Datye, M. Neurock, R.J. Davis, J.A. Dumesic, J. Am. Chem. Soc. 133 (2011) 12675–12689.
[38] S.P. Burt, K.J. Barnett, D.J. McClelland, P. Wolf, J.A. Dumesic, G.W. Huber, I. Hermans, Green Chem. 19 (2017) 1390–1398.
[39] A. Said, D. Da Silva Perez, N. Perret, C. Pinel, M. Besson, ChemCatChem 9 (2017) 2768–2783.
[40] A. Allgeier, N. Desilva, E. Korovessi, C. Menning, J.C. Ritter, S.K. Sengupta, Process for preparing 1,6-hexanediol, WO Pat. 2013/101980 (2013), to E.I. Du Pont de Nemours and Company.
[41] S.H. Krishna, D.J. McClelland, Q.A. Rashke, J.A. Dumesic, G.W. Huber, Green Chem. 19 (2017) 1278–1285.
[42] M. Faber, Process for producing adipic acid from biomass, US Pat. 1983/4400468 (1983), to Hydrocarbon Research.
[43] M.S. Ide, R.J. Davis, J. Catal. 308 (2013) 50–59.
[44] M.S. Ide, D.D. Falcone, R.J. Davis, J. Catal. 311 (2014) 295–305.
[45] T. Wang, M.S. Ide, M.R. Nolan, R.J. Davis, B.H. Shanks, Energy Environ. Focus 5 (2016) 1–5.
[46] J. Xie, B. Huang, K. Yin, H.N. Pham, R.R. Unocic, A.K. Datye, R.J. Davis, ACS Catal. 6 (2016) 4206–4217.
[47] E.L. Dias, V.J. Murphy, J.A.W. Shoemaker, Process for production of adipic acid from 1,6-hexanediol, US Patent2013/0331606 (2013), to Rennovia.
[48] S.E. Davis, M.S. Ide, R.J. Davis, Green Chem. 15 (2013) 17–45.
[49] M. Besson, P. Gallezot, Catal. Today 57 (2000) 127–141.
[50] M. Besson, F. Lahmer, P. Gallezot, P. Fuertes, G. Fleche, J. Catal. 152 (1995) 116–121.
[51] H. Ait Rass, N. Essayem, M. Besson, Green Chem. 15 (2013) 2240–2251.
[52] J. Xie, D.D. Falcone, R.J. Davis, J. Catal. 332 (2015) 38–50.
[53] A. Lolli, S. Albonetti, L. Utili, R. Amadori, F. Ospitali, C. Lucarelli, F. Cavani, Appl. Catal. A: Gen. 504 (2015) 408–419.
[54] C.L. Bianchi, P. Canton, N. Dimitratos, F. Porta, L. Prati, Catal. Today 102 (2005) 203–212.
[55] D.I. Enache, J.K. Edwards, P. Lanton, B. Solsona-Espriu, A.F. Carley, A.A. Herzing, M. Watanabe, C.J. Kiely, D.W. Knight, G.J. Hutchings, Science 311 (2006) 362–365.
[56] A. Villa, D. Wang, D. Su, G.M. Veith, L. Prati, Phys. Chem. Chem. Phys. 12 (2010) 2183–2189.
[57] W. Hou, N.A. Dehm, R.W.J. Scott, J. Catal. 253 (2008) 22–27.
[58] N. Dimitratos, J.A. Lopez-Sanchez, G.J. Hutchings, Chem. Sci. 3 (2012) 20–44.
[59] P. Korovchenko, C. Donze, P. Gallezot, M. Besson, Catal. Today 121 (2007) 13–21.
[60] M. Simões, S. Baranton, C. Coutanceau, Appl. Catal. B: Environ. 110 (2011) 40–49.
[61] A.-B. Crozon, M. Besson, P. Gallezot, New J. Chem. 22 (1998) 269–273.
[62] K. Heidkamp, M. Aytemir, K.-D. Vorlop, U. Prüesse, Catal. Sci. Technol. 3 (2013) 2984–2992.
[63] C. Louis, Catalysts 6 (2016) 110–136.
[64] E. Derrien, P. Marion, C. Pinel, M. Besson, Ind. Eng. Chem. Res. (2017), http://dx.doi.org/10.1021/acs.iecr.7b01571.
[65] K. Laaziri, S. Roorda, J. Baribeau, J. Non-Cryst. Solids 191 (1995) 193–199.
[66] H. Miura, K. Endo, R. Ogawa, T. Shishido, ACS Catal. 7 (2017) 1543–1553.
[67] T. Mallat, A. Baiker, Chem. Rev. 104 (2004) 3037–3058.
[68] A. Abad, P. Concepción, A. Corma, H. García, Angew. Chem. Int. Ed. 44 (2005) 4066–4069.
[69] L. Prati, P. Spontoni, A. Gaiassi, Top. Catal. 52 (2009) 288–296.
[70] A. Villa, D. Wang, N. Dimitratos, D. Su, V. Trevisan, L. Prati, Catal. Today 150 (2010) 8–15.
[71] N. Dimitratos, A. Villa, D. Wang, F. Porta, D. Su, L. Prati, J. Catal. 244 (2006) 113–121.
[72] B.N. Zope, S.E. Davis, R.J. Davis, Top. Catal. 55 (2012) 24–32.
[73] T. Balcha, J.P. Strobl, C. Fowler, P. Dash, R.W.J. Scott, ACS Catal. 1 (2011) 425–436.
[74] X. Wan, C. Zhou, J. Vhen, W. Deng, Q. Zhang, Y. Yang, Y. Wang, ACS Catal. 4 (2014) 2175.
[75] Y. Ryabenkova, P.J. Miedziak, D.W. Knight, S.H. Taylor, G.J. Hutchings, Tetrahedron 70 (2014) 6055–6058.